Article

Neuron

Non-canonical Wnt Signaling through *Ryk* Regulates the Generation of Somatostatin- and Parvalbumin-Expressing Cortical Interneurons

Highlights

- Rostral and caudal subdomains of the MGE differentially produce PV and SST interneurons
- Wnt/Ryk signaling is required to establish MGE subdomains
- Ryk genetic loss of function results in gross misspecification of cortical interneurons
- *In vitro* activation of the Ryk pathway regulates ES differentiation to PV and SST cells

Authors

Melissa G. McKenzie, Lucy V. Cobbs, Patrick D. Dummer, ..., Yimin Zou, Gord J. Fishell, Edmund Au

Correspondence

ea2515@cumc.columbia.edu

In Brief

Non-canonical Wnt signaling through the Ryk receptor establishes regional subdomains within the MGE along the rostral-caudal axis. These subdomains are defined by graded Ryk signaling, which regulates the proportions of parvalbumin and somatostatin cortical interneurons produced during development.

McKenzie et al., 2019, Neuron *103*, 853–864
September 4, 2019
https://doi.org/10.1016/j.neuron.2019.06.003

CellPress

Neuron
Article

Non-canonical Wnt Signaling through *Ryk* Regulates the Generation of Somatostatin- and Parvalbumin-Expressing Cortical Interneurons

Melissa G. McKenzie,[1,2] Lucy V. Cobbs,[2] Patrick D. Dummer,[1] Timothy J. Petros,[2,9] Michael M. Halford,[3] Steven A. Stacker,[3] Yimin Zou,[4] Gord J. Fishell,[2,5,6] and Edmund Au[1,2,7,8,10,*]
[1]Department of Pathology and Cell Biology, Columbia University Medical Center, New York, NY 10032, USA
[2]NYU Neuroscience Institute, New York University Langone Medical Center, New York, NY 10016, USA
[3]Tumour Angiogenesis and Microenvironment Program, Department of Oncology, Peter MacCallum Cancer Centre, 305 Grattan St, Melbourne, Victoria 3000, Australia
[4]Neurobiology Section, Biological Sciences Division, University of California, San Diego, CA 92093, USA
[5]Department of Neurobiology, Harvard Medical School, Boston, MA 04115, USA
[6]The Stanley Center at the Broad, Cambridge, MA 02142, USA
[7]Department of Rehabilitation and Regenerative Medicine, Columbia University Medical Center, New York, NY 10032, USA
[8]Columbia Translational Neuroscience Initiative Scholar, Columbia University Medical Center, New York, NY 10032, USA
[9]Present address: Eunice Kennedy-Shriver National Institutes of Child Health and Human Development, National Institutes of Health, Bethesda, MD 20892, USA
[10]Lead Contact
*Correspondence: ea2515@cumc.columbia.edu
https://doi.org/10.1016/j.neuron.2019.06.003

SUMMARY

GABAergic interneurons have many important functions in cortical circuitry, a reflection of their cell diversity. The developmental origins of this diversity are poorly understood. Here, we identify rostral-caudal regionality in Wnt exposure within the interneuron progenitor zone delineating the specification of the two main interneuron subclasses. Caudally situated medial ganglionic eminence (MGE) progenitors receive high levels of Wnt signaling and give rise to somatostatin (SST)-expressing cortical interneurons. By contrast, parvalbumin (PV)-expressing basket cells originate mostly from the rostral MGE, where Wnt signaling is attenuated. Interestingly, rather than canonical signaling through β-catenin, signaling via the non-canonical Wnt receptor Ryk regulates interneuron cell-fate specification *in vivo* and *in vitro*. Indeed, gain of function of Ryk intracellular domain signaling regulates SST and PV fate in a dose-dependent manner, suggesting that Ryk signaling acts in a graded fashion. These data reveal an important role for non-canonical Wnt-Ryk signaling in establishing the correct ratios of cortical interneuron subtypes.

INTRODUCTION

Interneurons provide inhibitory tone and play critical roles in brain function: regulating cortical rhythmicity, attention states, and signal timing (Cardin et al., 2009; Fino and Yuste, 2011; Kvitsiani et al., 2013; Lapray et al., 2012). The majority of interneurons are contained within one of two broad cardinal classes: parvalbumin (PV)- and somatostatin (SST)-expressing cell types, which are fundamentally distinct in terms of their connectivity and contribution to brain function (Fishell and Rudy, 2011). The former type is perisomal or axonal targeting, is fast spiking, and shows synaptic depression (Hu et al., 2014; Inan et al., 2013; Taniguchi et al., 2013), whereas the latter provides inhibition to dendrites, is regular spiking, and typically displays synaptic facilitation (Lovett-Barron et al., 2012). Despite these differences, PV+ and SST+ interneurons originate from the same embryonic structure, the medial ganglionic eminence (MGE).

Understanding how functionally distinct cell types arise from a common origin remains a fundamental challenge. We have previously proposed that this process is essentially accomplished in two phases, "cardinal specification" into major subclasses followed by "definitive specification" of mature functional properties as they integrate into cortical circuitry (Kepecs and Fishell, 2014; Wamsley and Fishell, 2017). With respect to definitive specification, significant progress has been made in identifying extrinsic and intrinsic factors that act coordinately with neuronal activity to differentially fine-tune granular properties of interneurons (De Marco García et al., 2011, 2015; Dehorter et al., 2015). Furthermore, intrinsic regulation of interneuron identity by transcriptional regulation has been extensively studied (Wonders and Anderson, 2006). However, a conclusive extrinsic mechanism underlying cardinal specification is presently lacking. Previous findings have implicated multiple secreted growth factors, notably sonic hedgehog (Shh), and key transcription factors for both the initial acquisition and later maintenance of cardinal identity (Anderson et al., 1997; Sussel et al., 1999; Tyson et al., 2015; Xu et al., 2010). Furthermore, there is evidence of spatial heterogeneity in the types of interneurons generated from different regions of the MGE (Flames et al., 2007; Hu et al., 2017; Wonders

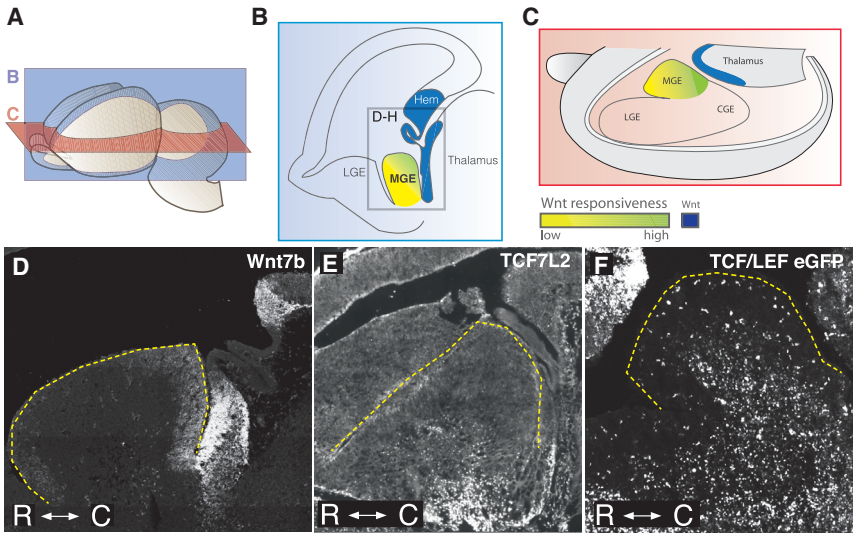

Figure 1. Expression of Wnt Signaling Factors Present near the Medial Ganglionic Eminence at Embryonic Day 13.5

(A) Planes of section for (B) and (C) in relation to a whole E13.5 brain.

(B) Parasagittal schematic of E13.5 caudal Wnt sources and Wnt responsiveness across the MGE. Box denotes cropped region for *in situ* hybridization images in (D)–(F).

(C) Schematic diagram in the transverse plane showing the same spatial relationship of caudal Wnt sources and Wnt responsiveness across the MGE.

(D) *In situ* hybridization of Wnt7b.

(E) Tcf7l2 immunostaining for Tcf7l2 protein, an early readout for canonical Wnt signaling. Tcf7l2-positive cells in the mantle are enriched in the caudal portion of the MGE.

(F) Horizontal section of MGE in Tcf/Lef:H2B-dGFP reporter animals at E13.5. eGFP expression is enriched in the caudal MGE. The outline of the MGE is denoted by the yellow dashed line.

et al., 2008, Hu et al., 2017). Moreover, during development, the proportion of subtypes produced shifts; SST+ cells are preferentially generated earlier, with the production of PV+ cells predominating at later developmental time points (Inan et al., 2012; Miyoshi et al., 2007). Therefore, a model to explain the precise orchestration of PV+ versus SST+ cardinal specification must (1) account for the bias in spatial origins between the two subtypes, (2) cleanly delineate between PV+ and SST+, and (3) explain the proportional shift in subtype production over time.

Here we describe regional variability in Wnt responsiveness along the caudal-rostral axis of the MGE that reflects Wnt sources emanating from caudally situated embryonic structures. Transplants of MGE subdomains along this axis reveal a strong bias in the spatial origin of PV+ and SST+ cells such that strongly Wnt-responsive cells become SST+ interneurons and lower levels of Wnt produce PV+ cells. We demonstrate that Ryk signaling, which has been described in a number of biological contexts (Roy et al., 2018), is at least partially responsible for the delineation between PV+ and SST+ cell fate, independent of canonical Wnt signaling through β-catenin or Shh signaling. Genetic ablation of *Ryk* compromises the ability of nearly half of cells to acquire PV+ and SST+ interneuron identity; the remaining cells no longer exhibit a population bias for PV+ over SST+. We further show that Ryk signaling is dynamically regulated throughout development and parallels the differential production of SST+ and PV+ interneurons over time. Indeed, the proportion of SST+ and PV+ interneurons can be regulated in an *in vitro* model of interneuron development (Au et al., 2013) by directly modulating Ryk signaling. Therefore, Ryk signaling is a critical component of interneuron cardinal specification that controls the relative proportions of PV+ and SST+ subtypes produced and thus enables proper microcircuit assembly.

RESULTS

Previous work has shown that the initial specification of interneuron subtype identity is determined at the progenitor phase, prior to the exit from the cell cycle (Butt et al., 2005; Inan et al., 2012; Nery et al., 2002; Taniguchi et al., 2013; Wichterle et al., 2001). In a variety of developmental contexts, morphogen gradients have been shown to create variation and diversity within progenitor fields, a process most thoroughly studied with regard to Shh signaling in the spinal cord (Briscoe and Ericson, 2001; Dessaud et al., 2007; Ericson et al., 1997; Roelink et al., 1995). Similarly, a number of studies have indicated that Shh signaling within the MGE also biases interneuron subtype identity (Flames et al., 2007; Inan et al., 2013; Puelles and Rubenstein, 2003; Rubenstein et al., 1994; Taniguchi et al., 2013; Wonders et al., 2008). However, a role for other morphogens in the production of PV+ or SST+ cells from the MGE remains elusive.

Expression of Wnt Signaling Components Suggests a Caudal-to-Rostral Gradient across the MGE

Wnt has been found to play an important role in the expansion of the subventricular zone within the MGE (Gulacsi and Anderson, 2008) and the PV^+ interneurons that preferentially arise from this proliferative area (Glickstein et al., 2007; Gulacsi and Anderson, 2008; Petros et al., 2015). This led us to investigate whether Wnt might play additional roles in patterning the MGE by providing graded signaling, as has been described elsewhere in the nervous system (Charron and Tessier-Lavigne, 2005; Lee and Jessell, 1999). Using publicly available CNS gene expression data from the Allen Institute, we performed an *in silico* screen and found that multiple Wnt ligands are expressed in close proximity to the MGE (Figure 1; Figure S1) (http://developingmouse.brain-map.org). Caudal to the MGE, *Wnt7a* and *Wnt7b* are both highly expressed in the superficial stratum of the prethalamic eminence as well as in the cortical hem (Figure 1D; Figure S1), where *Wnt3a* and *Wnt5a* are also expressed (Figure S1). *Tcf7l2*, a canonical Wnt-responsive transcription factor, is also present in the caudal aspect of the MGE mantle, where newborn interneurons begin their migration (Figure 1E). A Wnt reporter mouse expressing a destabilized histone 2B-eGFP fusion protein under the control of general Tcf/Lef promoter

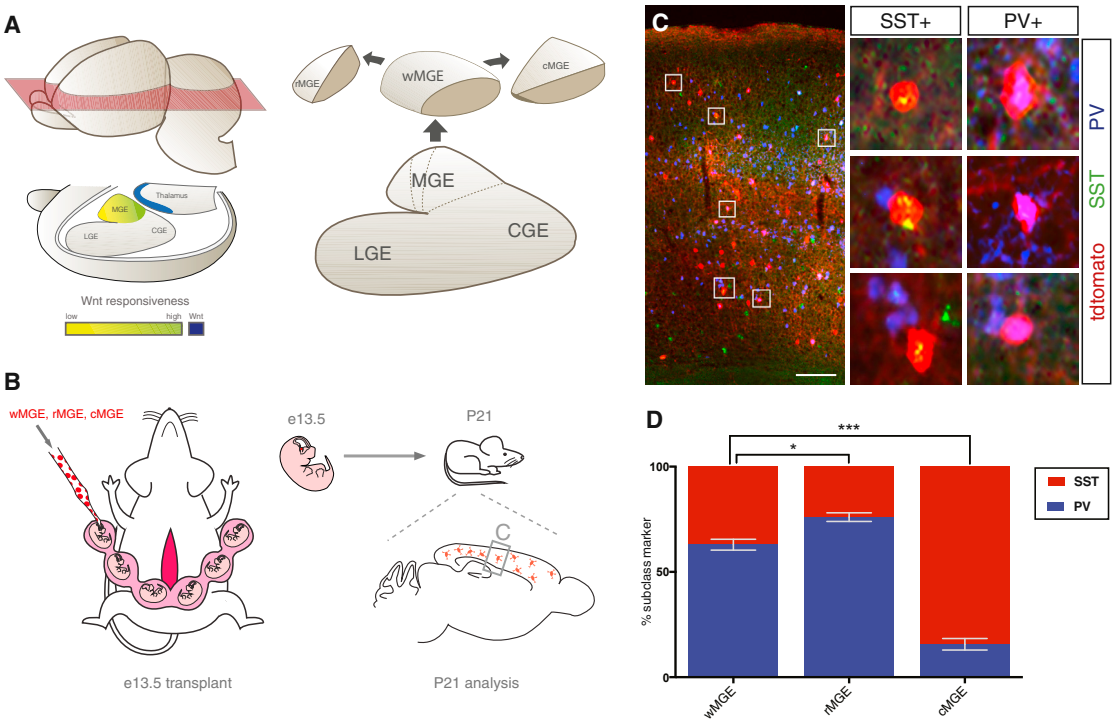

Figure 2. Ultrasound-Guided *In Utero* Transplantation to Determine the Cortical Interneuron Output of MGE Subdomains

(A) Schematic diagram of spatial relationship between Wnt source (blue) and Wnt responsiveness within the MGE (green to yellow) suggests the presence of MGE subdomains along the rostral caudal axis. Whole (wMGE), rostral (rMGE), and caudal (cMGE) were dissected for transplantation studies.

(B) Schematic of transplantation experiment. Pan-RFP-expressing w-, r-, and cMGE were transplanted into E13.5 mouse MGE in separate experiments by ultrasound backscatter microscopy. Host mice were sacrificed 27 days post-transplant (postnatal day 21 [P21]), and donor cortical interneurons were analyzed for SST+ and PV+ expression.

(C) Representative coronal section of P21 host forebrain showing RFP+ donor cells engrafted in cortex (scale bar, 200 μm). Middle panel is higher magnification of box on left; boxes 1–6 show high-power images of transplanted cells positive for RFP and either SST or PV.

(D) P21 analysis of w-, r-, and cMGE transplantation studies for SST+ and PV+ expression in transplanted interneurons. Error bars, SEM (*$p < 0.05$; **$p < 0.01$; ***$p < 0.001$).

elements (Ferrer-Vaquer et al., 2010) (*Wnt reporter*) also shows enriched eGFP expression in the caudal aspect of the MGE, suggestive of a caudal-high, rostral-low Wnt gradient of responsiveness within the MGE (Figures 1F and 3A). Within the rostral aspect of the MGE, the Wnt antagonist *Sfrp1* (Secreted frizzled receptor protein 1) is expressed (Figure S2). Upon further investigation of genes with similar enrichment in the MGE to *Nkx2-1*, we discovered that a large number of genes display a caudal-rostral divergence in their expression pattern (Figure S2). We therefore hypothesized that this regionality may arise from differences in exposure to Wnt ligands, resulting in signaling gradients that underlie previously described regional variation in generation of interneuron cell types (Wonders et al., 2008; Flames et al., 2007; Hu et al., 2017).

The Rostral and Caudal MGE Give Rise to Different Interneuron Subclasses

Our lab has previously employed ultrasound backscatter microscopy (UBM) as a means of grafting donor ventral eminence tissue into specific substructures of host embryonic brain. Through such fate mapping, we demonstrated that donor eGFP+ MGE cells, when transplanted into wild-type recipient host MGE, migrate dorsally and integrate throughout the cortex alongside endogenous interneurons (Butt et al., 2005; Nery et al., 2002; Wichterle et al., 2001). To directly examine whether rostral versus caudal MGE (rMGE and cMGE, respectively)-derived cortical interneurons assume different fates within the cortex, we used a similar UBM transplantation approach (Figure 2). From embryos ubiquitously expressing tdTomato, the caudal (high Wnt) and rostral (low Wnt) portions of embryonic day 12.5 (E12.5) MGEs were microdissected and transplanted into the MGE of E13.5 unlabeled host embryos (Figures 2A and 2B; Figure S3). Brains from animals receiving grafts were collected at postnatal day 21 (P21) when interneuron progenitors have fully matured. Transplanted cells were scored for expression of SST or PV by immunohistochemistry (Figure 2C). Compared to control transplants of the whole MGE (wMGE), rMGE and cMGE transplants were strongly biased for PV and SST, respectively (wMGE n = 8, 63% PV and 37% SST of identified cells, SD 4.5%, 25% unidentified of all labeled cells, rMGE n = 14, 71% PV and 29% SST of identified cells, 29% unidentified of all labeled cells, SD 7.3%, cMGE n = 4, 16% PV and 84% SST of identified cells, SD 2.4%, 23% unidentified of all labeled cells, chi-square test p value = 0.02, 0.0001, Figure 2D).

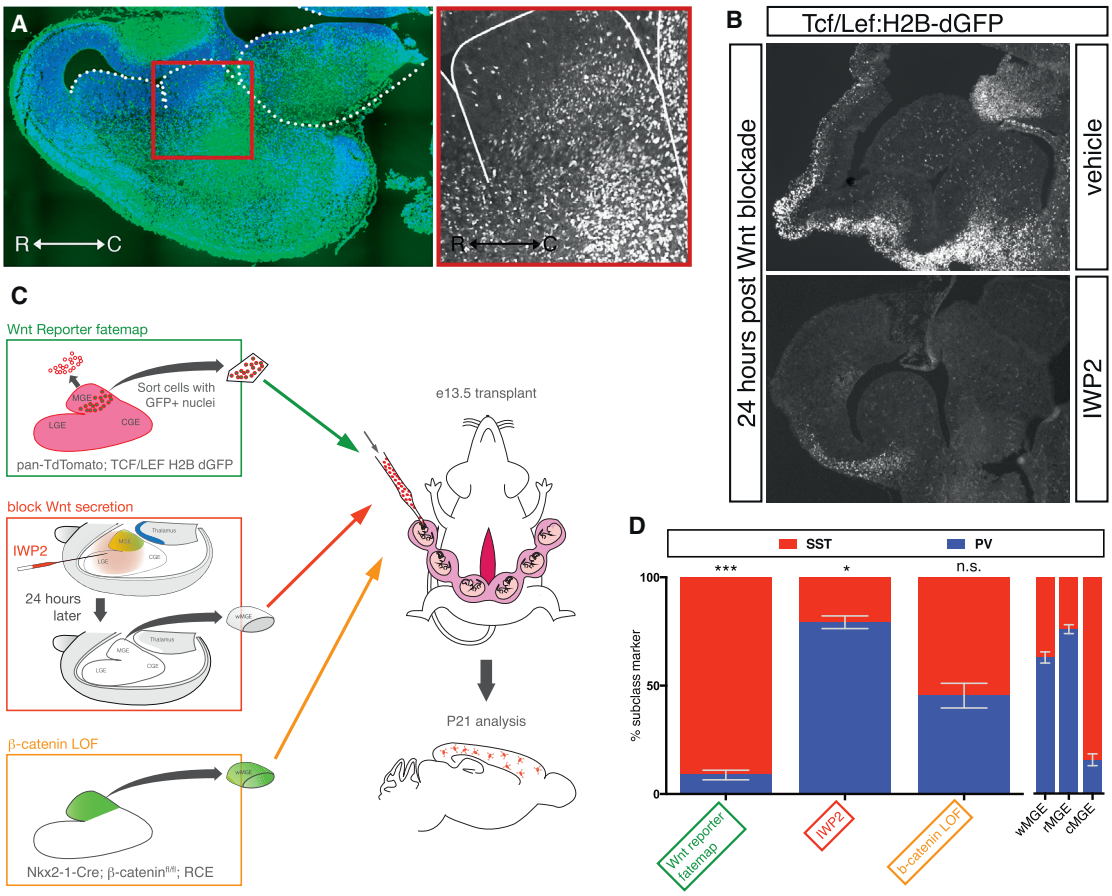

Figure 3. Exploring the Role of Wnt Signaling in Determining Cortical Interneuron Subtype Identity

(A) Transverse section of E13.5 mouse brain in Tcf/Lef:H2B-dGFP reporter mouse. Nuclear GFP is enriched in caudal portion of MGE.

(B) Parasagittal section of Tcf/Lef:H2B-dGFP reporter mouse at E13.5 showing regions of Wnt responsiveness. 24 h after intraventricular injection of vehicle did not affect GFP signal. 24 h following intraventricular injection of IWP2 strongly reduced GFP signal.

(C) Schematic diagram depicting the different transplant studies performed to examine the role of Wnt in interneuron specification. Green box shows pan-RFP+ cells sorted for eGFP+ nuclei indicative of Wnt responsiveness. Red box shows intraventricular injection of IWP2 at E12.5, followed by dissection and transplant of wMGE 24 h post injection. Orange box shows genetic removal of β-catenin and simultaneous eGFP+ fate mapping of MGE prior to dissection and transplantation.

(D) P21 analysis of studies transplanting Tcf/Lef:H2B-dGFP+ MGE cells, blocking Wnt secretion prior to transplantation, or genetically removing β-catenin in transplanted MGE. w-, r-, and cMGE transplant results on right for comparison. Error bars, SEM (*$p < 0.05$; **$p < 0.01$; ***$p < 0.001$).

Fate-Mapped Wnt-Responsive Cells Are Biased toward Production of SST+ Interneurons

Since the presence of SST+ cells was strikingly enriched in the cMGE, we sought to establish a more direct relationship between Wnt responsiveness in MGE progenitors and SST+ cell fate. To do so, we made use of the histone 2B-eGFP *Wnt reporter* mouse mentioned above (Figures 1F and 3A) (Ferrer-Vaquer et al., 2010). In order to both identify cells that receive strong Wnt signaling at E12.5 and characterize them as they achieve their mature fate, we crossed the Wnt reporter onto a background ubiquitously expressing tdTomato. We then dissected MGEs from E12.5 embryos and used flow cytometry to capture cells with high levels of nuclear eGFP expression, indicating high levels of Wnt signaling activity (Figure 3C, green box; Figure S3). After transplanting flow cytometry-isolated nuclear eGFP+ cells into unlabeled hosts, transplanted cells, marked by their expression of tdTomato, were scored for marker expression at P21. Overwhelmingly, embryonic progenitors with high levels of Wnt activity gave rise to SST+ cells (Figure 3D) (9% PV+ and 91% SST+ of identified cells, 18% unidentified cells of total reporter labeled cells, n = 2, compared to wMGE p = 0.0003, unpaired Student's t test).

Wnt Inhibition Decreases SST+ Interneuron Production

In order to establish a causal link between Wnt signaling and interneuron identity, we administered IWP2, a small molecule inhibitor of the membrane-bound O-acyl transferase (MBOAT) protein Porcupine (Porcn) (Chen et al., 2009). Porcupine is essential for the post-translational acylation and secretion of all secreted Wnts (Barrott et al., 2011; Proffitt and Virshup, 2012; Willert et al., 2003). Indeed, IWP2 injection into the ventricle of E12.5 *Wnt reporter* mice dramatically reduced Wnt reporter expression within 24 h (Figures 3A and 3B). We hypothesized that a reduction in Wnt signaling would mimic an expansion of

the low Wnt rostral MGE and result in a proportional decrease of SST+ cells. To test this, we injected the ventricles of fluorescently labeled mice with IWP2 at E12.5 and collected MGE tissue 24 h later for transplantation into E13.5 host embryos (Figure 3A, red box). When we analyzed hosts at P21, we found that a reduction in Wnt signaling resulted in a dramatic increase of interneurons that adopted a PV+ fate compared to wMGE transplants (Figure 3D) (79% PV+ and 21% SST+, of identified cells, 27% unidentified cells of total reporter expressing cells, n = 4, p = 0.03 unpaired Student's t test compared to wMGE).

Canonical Wnt Signaling Does Not Significantly Influence Cell Fate

Canonical Wnt signaling requires the intracellular signaling molecule β-catenin. Under basal conditions, β-catenin is sequestered within the cytoplasm and targeted for degradation by GSK3-β. Binding of Wnt ligand to the Frizzled (FZD) family of Wnt receptors prevents β-catenin degradation, resulting in its accumulation and translocation to the nucleus where it initiates the expression of Tcf/Lefs to modulate gene expression (Cadigan and Waterman, 2012; reviewed in Willert and Nusse, 2012). Previous work suggests that loss of canonical Wnt signaling influences proliferation in the MGE (Gulacsi and Anderson, 2008). MGE-specific knockout of *β-catenin* is late-embryonic lethal, however, preventing assessment of the mature cell types produced from the mutant MGE. To circumvent this lethality and to determine whether disrupting Wnt signaling through *β-catenin* affects cell-type specification in the MGE, we generated E12.5 MGE-specific knockouts of *β-catenin* (Brault et al., 2001). This was achieved by crossing a conditional *β-catenin*$^{f/f}$ allele onto the *Nkx2.1*^{Cre} driver line and a conditional GFP reporter (Sousa et al., 2009; Xu et al., 2008). Embryonic mutants were identified by a midline fusion defect in the ventral forebrain, a phenotype characteristic of *β-catenin* loss of function in the MGE and confirmed by DNA genotyping after transplantation. Mutant MGEs were collected, dissociated, and transplanted into embryonic hosts (Figure 3B, orange box). Interestingly, analysis of this population at P21 showed that the loss of β-catenin signaling resulted in a non-significant trend toward SST+ cell production compared to wMGE (41% PV+ and 56% SST+ of identified cells, n = 3, p = 0.1 paired Student's t test compared to wMGE, 25% unidentified). The opposing effect between *β-catenin* loss and Wnt inhibition lead us to consider the role of non-canonical Wnt signaling pathways.

Non-canonical Wnt Receptor, Ryk, Is Preferentially Active in cMGE

Wnt signals through a number of β-catenin-independent pathways, including the planar cell polarity and convergent extension pathways, as well as non-FZD receptors including Ryk, Ror1, and Ror2 (Green et al., 2014). To identify the most promising candidates mediating non-canonical Wnt signaling within the MGE, we measured the expression levels of a number of non-canonical Wnt signaling genes in E13.5 MGE by RT-PCR. Many non-canonical Wnt signaling components were expressed at negligible levels; the exceptions being Vangl2, a membrane protein important for the planar cell polarity pathway, and Ryk, a receptor-like tyrosine kinase that binds Wnt (Figure 4A). Forebrain-specific knockouts of *Vangl2* are viable throughout adulthood and display no phenotypes suggestive of MGE interneuron deficits such as seizures (Qu et al., 2014; A. Goffinet, personal communication). By contrast, Ryk has been shown to have a role in cortical neurogenesis and MGE cell production; *Ryk*$^{-/-}$ animals are perinatal lethal, which has precluded analysis of which interneuron subtypes are affected (Lyu et al., 2008; Zhong et al., 2011).

Ryk signaling in cortical neurogenesis occurs via the cleavage and nuclear translocation of the intracellular portion of the Ryk receptor (Lyu et al., 2008). Cleavage of the Ryk receptor by γ-secretase is constitutive and independent of Wnt signaling (Lyu et al., 2008). Through an unknown mechanism, the presence of Wnt ligand is thought to induce the translocation of the cleaved Ryk intracellular domain (Ryk ICD) from the cytoplasm to the nucleus (Lyu et al., 2008). In order to establish whether Ryk signaling was differentially active in the rMGE versus cMGE, we compared protein from pooled samples of rostral and caudal MGE (Figure 4B). We fractionated protein samples from the r-, c-, and wMGE into whole-cell, cytoplasmic, and nuclear fractions and assessed Ryk activation by Ryk ICD levels in the nucleus. By western blot, we found Ryk ICD to be enriched in the nuclear fraction of the cMGE compared to the rMGE (Figures 4C and 4E), indicating that Ryk receptor activation aligns with the predicted regionality of Wnt exposure. Our previous experiments indicated that inhibition of Wnt by IWP2 treatment both significantly decreases the amount of canonical Wnt signaling by the Tcf/Lef eGFP reporter activation and the number of SST+ interneurons produced (Figures 3B and 3D). Consistent with prior reports that Ryk ICD signaling (Lyu et al., 2008) is modulated by Wnt, we found that MGEs treated with the Wnt inhibitor IWP2 for 24 h showed a significant decrease in Ryk ICD signal in the cytoplasmic fraction compared with vehicle-treated controls (Figures 4D and 4G). Full-length Ryk receptor signal was also decreased in IWP2-treated MGE samples (Figure 4F).

During development, the proportions of PV+ and SST+ interneurons produced by the MGE change. While SST+ interneurons are strongly enriched in early cohorts, the production of PV+ interneurons predominates during later stages of embryonic development. We therefore examined presence of nuclear Ryk ICD in wMGE across developmental ages (E11.5 to E15.5). We observed a peak of nuclear Ryk ICD at E12.5 that declined at later ages (Figure 4H), consistent with the dynamic output of SST+ and PV+ interneurons over time. Furthermore, *in situ* hybridization of Ryk shows a decline in expression in the MGE with developmental age (Figure 4J). Wnt7a and -7b expression in the thalamus and hem also decline at later stages (Figure S1) (http://developingmouse.brain-map.org). These data demonstrate that Wnt ligands, Ryk expression, and the presence of nuclear Ryk ICD all decline during periods of reduced SST+ interneuron production and are consistent with the hypothesis that they are coordinately regulated.

Ryk Signaling Regulates SST+ and PV+ Generation Embryonically

We observed Ryk ICD signaling to be enriched in the caudal MGE, coincident with SST+ interneuron production. To test the sufficiency of activating Ryk signaling in SST fate specification,

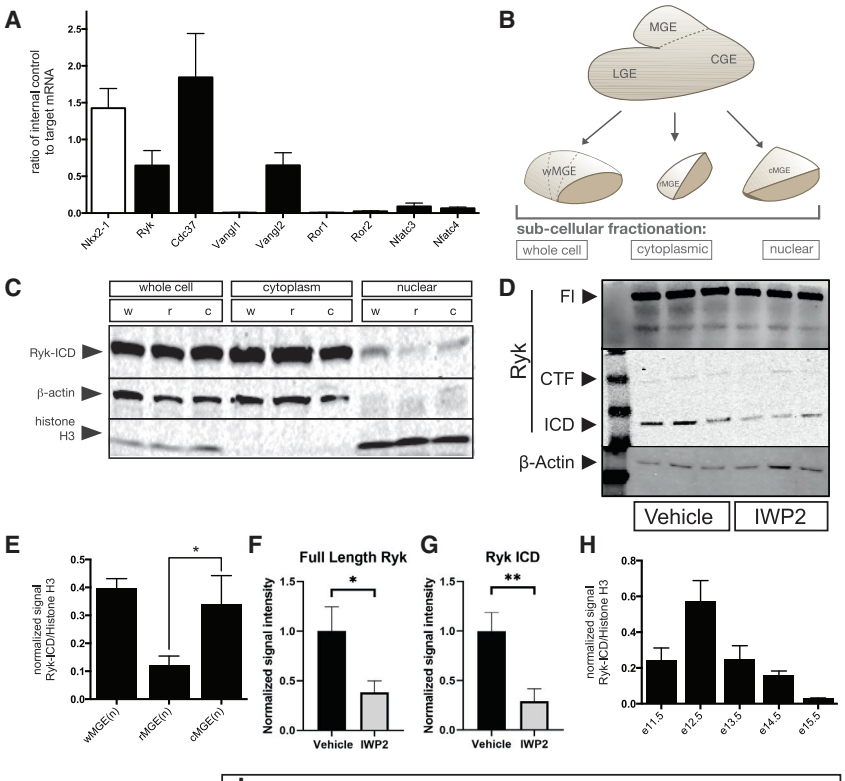

Figure 4. Identifying Components of Non-canonical Wnt and Ryk Signaling in the Embryonic MGE

(A) Quantitative PCR of E12.5 MGE for non-canonical Wnt signaling components. Nkx2-1 shown as a positive control.

(B) Schematic depiction of various MGE samples loaded for western blot in (C). See also Figure S3.

(C) Biochemical fractionations of w-, r-, and cMGE into whole-cell, cytoplasmic, and nuclear components were analyzed by western blot for Ryk, β-actin, and histone H3 (latter two act as loading controls).

(D) FL Ryk and Ryk ICD fragments are decreased in the cytoplasm of MGE cells 24 h after IWP2 treatment.

(E) Quantitation of blot in (C). Nuclear Ryk intracellular domain (Ryk-ICD) present in w-, r-, and cMGE samples.

(F and G) Quantification of Ryk full-length (F) and intracellular domain (G) protein fragments in blot shown in (D), normalized to loading control and average signal intensity of the vehicle-treated bands.

(H) wMGE nuclear fractions at various embryonic time points showing that Ryk signaling is dynamic over time.

(I and J) Schematic of parasagittal sections of 13.5 mouse brain (I). Equivalent areas at E11.5, E13.5, and E15.5 show decreasing levels of Ryk receptor over developmental time by (J) *in situ* hybridization for Ryk.

we utilized a previously employed Ryk gain-of-function strategy (Lyu et al., 2008). To do so, we generated a Cre-recombinase-dependent plasmid expressing the intracellular portion of the Ryk receptor tethered to a nuclear localization signal, as has been used previously to mimic constitutive Wnt-independent Ryk activation (nls-Ryk ICD) (Lyu et al., 2008). Electroporation of this plasmid into the MGE of *Nkx2.1*^{Cre} embryos at E12 resulted in a significant increase in the number of SST+ cells (compared to electroporation of control plasmid) produced in the electroporated cohort when assessed at P21 (Figure 5A). A concomitant decrease in the amount of PV+ interneurons in these same experiments was also observed (Figure 5A, *RICD* n = 3, Control n = 3, chi-square test $p \leq 0.0001$).

A previous study examining *Ryk*$^{-/-}$ embryos observed decreased MGE interneuron production and an increase in oligodendrogenesis (Zhong et al., 2011). However, the perinatal lethality of null animals prevented mature cortical interneuron subtype analysis. To circumvent this issue, we engrafted *Ryk*$^{-/-}$ MGE tissue into wild-type hosts to determine whether loss of *Ryk* affects the fate of interneurons in these mutants (Figure 5B). Ubiquitous tdTomato+;*Ryk*$^{+/-}$ animals were crossed, and at E12.5, *Ryk*$^{-/-}$ embryos were identified for dissection by PCR genotyping (see STAR Methods). Fluorescently labeled mutant MGEs were then transplanted into wild-type E13.5 host embryos for postnatal analysis. *Ryk*$^{-/-}$ transplants were capable of robust migration and integration into host cortex (Figure S4), but interestingly, the majority of *Ryk*$^{-/-}$ interneurons failed to fully differentiate as evidenced by the lack of mature cIN subtype marker expression, including CGE interneuron markers (Figure 5B) (50% unidentified, n = 2).

Eliminating *Ryk* entirely in the brain throughout development clearly has a marked effect on interneuron specification and production. As such, we wished to more precisely block Ryk function during a more restricted time window in order to examine the role of Ryk in PV+ and SST+ interneuron specification. To do so, we introduced a Ryk extracellular domain human function-blocking antibody (Halford et al., 2013) into the ventricles of E12 embryos. When analyzed at P21, animals treated with a Ryk function-blocking antibody had normal numbers of MGE-derived interneurons in the cortex but showed an ~15% increase in PV complemented by an ~15% decrease in SST numbers in the cortex, suggesting that Ryk blockade induced a fate switch (n = 4, unpaired Student's t test, p = 0.03, Figure S5).

Finally, in order to genetically ablate *Ryk* without perinatal lethality, we conditionally removed Ryk in the MGE while fate mapping the resulting mutant cells: *Nkx2-1*^{Cre}; Ai9; *Ryk*$^{f/f}$ with Nkx2-1^{Cre}; Ai9; Ryk$^{f/+}$ mice used as controls. At P21, nearly half (41.3%) of tdTomato+ cells did not express PV or SST (Figure 5C; Figure S5), oligodendrocyte, or CGE interneuron subtype

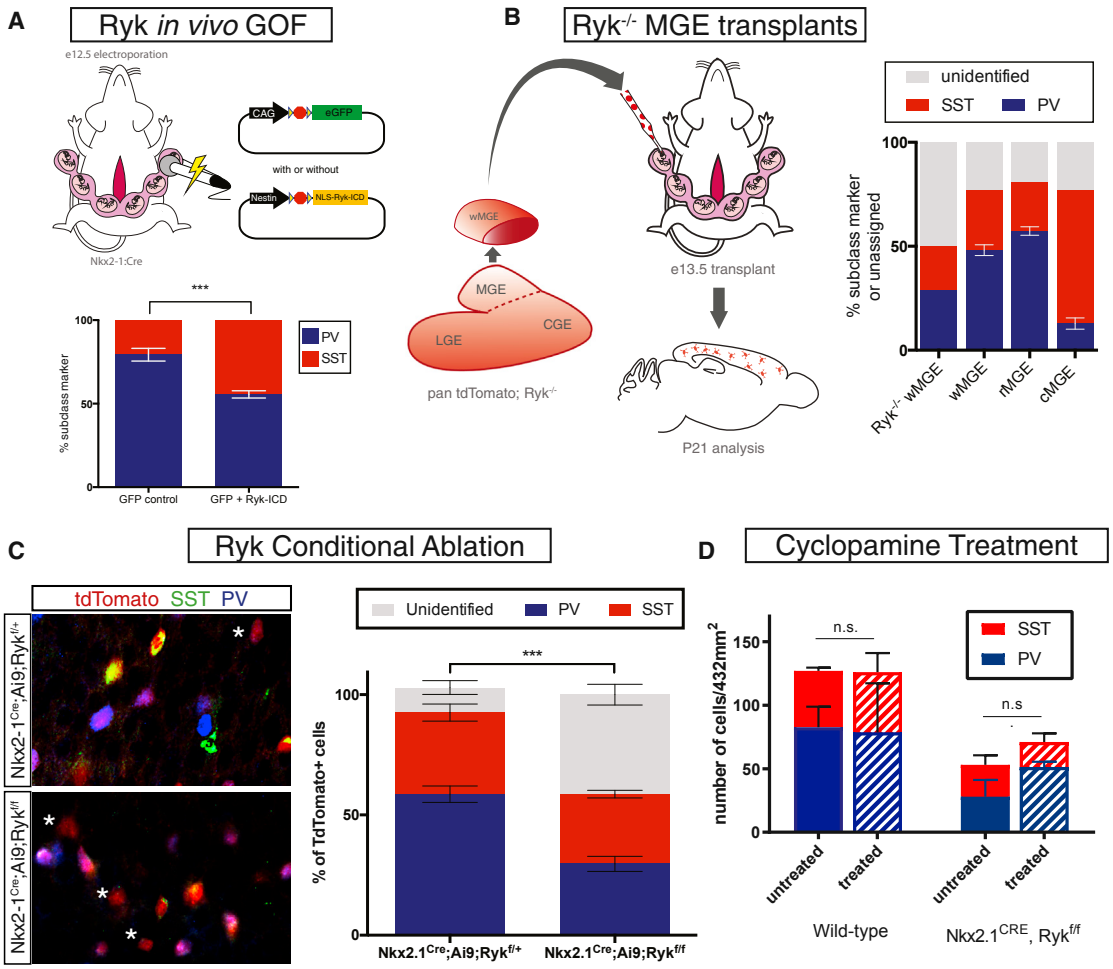

Figure 5. Ryk Loss and Gain of Function and Its Effects on Cortical Interneuron Specification

(A) Left: schematic diagram of electroporation paradigm for Ryk ICD gain of function in MGE progenitors. Right: analysis of PV+ and SST+ interneurons at P21 with control (GFP alone) or Ryk ICD gain-of-function (NLS-Ryk-ICD) plasmid electroporation. Ryk-ICD GOF resulted in a significant increase in SST+ and a decrease in PV+ electroporated interneurons.

(B) Left: schematic diagram showing $Ryk^{-/-}$ MGE transplant study. Right: P21 analysis revealed that $Ryk^{-/-}$ MGE transplants contain a large percentage of unidentified cortical interneurons; wild-type w-, r-, and cMGE transplant results for comparison.

(C) Conditional genetic ablation of *Ryk* and simultaneous labeling with tdTomato in the MGE using Nkx2-1^{Cre}. Left top: representative image of $Ryk^{f/+}$. Left bottom: representative image of $Ryk^{f/f}$. tdTomato in red, somatostatin in green, and parvalbumin in blue. Asterisks denote unidentified tdTomato+ cells. Right: quantification of unidentified somatostatin+ and parvalbumin+ tdTomato+ cells for each group. Error bars, SEM (*p < 0.05; **p < 0.01; ***p < 0.001).

(D) Treatment of $Nkx2.1^{Cre}$; $Ryk^{f/f}$ or WT embryos at E12.5 with cyclopamine has no significant or additive effect on the numbers of PV+ and SST+ interneurons observed in adults.

markers (Figure S6). Moreover, of the remaining tdTomato+ cells that expressed PV and SST (49.6% PV and 50.3% SST), there was no longer a population bias, whereas in controls, PV+ cells outnumbered SST+ cells (65.1% PV and 34.8% SST) (Figure 5C; Figure S6; controls n = 4, mutants n = 3, p = < 0.0001, chi-square test). The dramatic increase in unidentified cells raises the intriguing possibility that Ryk signaling is important for the maturation of interneurons. Postmitotic removal of Ryk from SST populations with SST^{Cre} or broadly using the postmitotic interneuron driver $Dlx6a^{Cre}$, however, resulted in no changes in interneuron marker expression (Figure S5). Taken together, these data strongly suggest that Ryk signaling regulates the generation of both PV+ and SST+ interneurons during the progenitor phase.

The reduction, but not complete loss, of PV and SST interneuron subtype markers when Ryk signaling is removed in MGE progenitors suggests alternate or redundant mechanisms to achieve interneuron subtype fate decisions. Shh signaling has previously been implicated in regional variation of interneuron production from the MGE, leading to the question as to whether Ryk and Shh pathways interact. To test whether Shh acts in parallel or in series with Ryk signaling, we injected the Shh antagonist cyclopamine into the ventricle of E12.5 $Nkx2.1^{Cre}$; $Ryk^{fl/+}$ and $Ryk^{fl/fl}$ embryos. We reasoned that if Shh is an alternative or redundant mechanism for MGE cell specification, then Shh blockade would result in an exacerbation of the Ryk mutant phenotype, perhaps leading to an increase in the

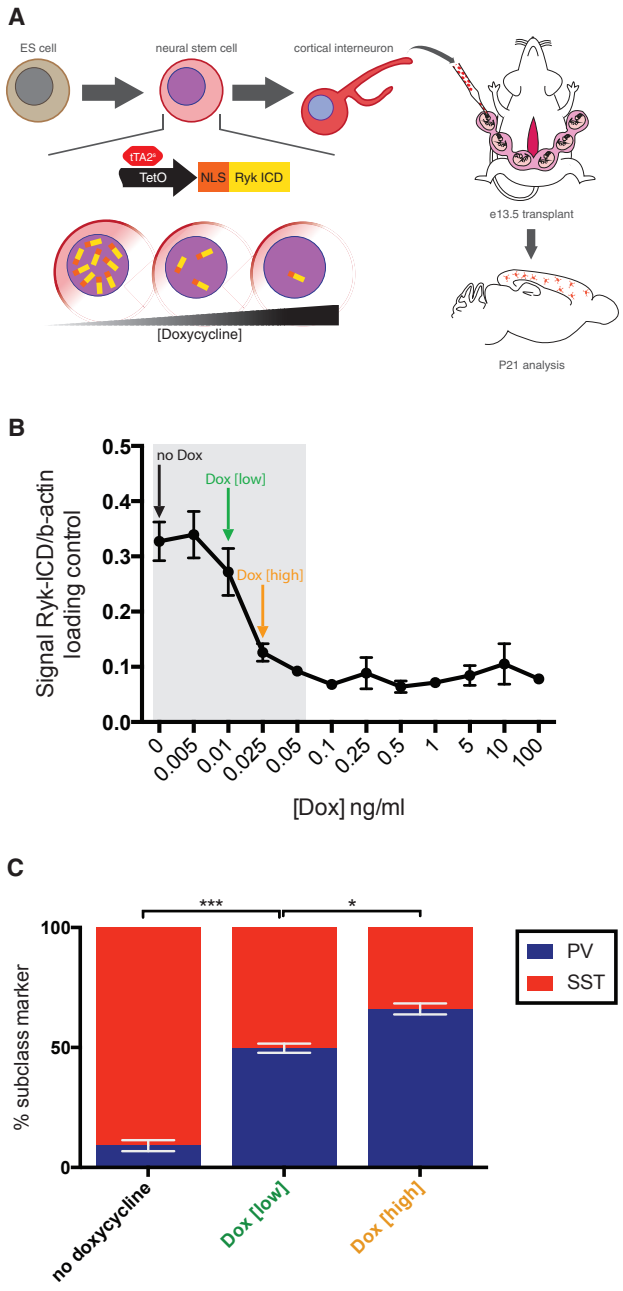

Figure 6. Investigating the Role of Graded Ryk Signaling in Interneuron Lineage Specification

(A) Schematic diagram of the regulation of tetracycline transactivator $tTA2^S$ by varying doxycycline added to medium during ES cell differentiation to interneuron. $tTA2^S$ activity regulates the graded expression of NLS-Ryk-ICD. After differentiation into interneurons, cells were transplanted by UBM at E13.5 and analyzed at P21 for SST+ and PV+ expression.

(B) Doxycycline dose response curve was determined empirically in order to ascertain appropriate low and high doxycycline concentrations for transplant experiments.

(C) Results of transplantation studies in which ES cells were differentiated in no, low, or high doxycycline concentrations. Error bars, SEM (*$p < 0.05$; **$p < 0.01$; ***$p < 0.001$).

number of unidentified (PV-negative, SST-negative) cells. Analysis at E13.5 revealed that cyclopamine treatment resulted in a decrease in expression of the Shh-responsive transcription factor Gli1 (Figure S5) in the MGE. However, P21 analysis of cyclopamine-treated animals did not demonstrate significant changes in PV+ or SST+ interneuron numbers in the cortex of treated mutants or controls (Figure 5D).

Graded Ryk Activation Regulates the Production of SST+ and PV+ Interneurons from Embryonic Stem Cells

Data from $Ryk^{-/-}$ transplants, Ryk conditional loss-of-function, and Ryk ICD gain-of-function experiments suggest that Ryk ICD signaling drives SST+ and is required for PV+ interneuron production. We observed high levels of nuclear Ryk ICD in the cMGE and low but detectable Ryk ICD in the rostral MGE. We also noted a gradual decrease in Ryk signaling in the MGE developmentally (Figure 4E). Taken together, these data suggest that Ryk acts in a graded, dose-dependent manner, where high Ryk signaling favors the production of SST+ interneurons and low Ryk signaling favors the production of PV+ interneurons. To directly test this hypothesis, we made use of an *in vitro* gain-of-function model system that we previously devised whereby mouse embryonic stem (ES) cells are transcriptionally specified to become cortical interneurons (Figure 6A) (Au et al., 2013). In the context of this system, we introduced a constitutively active form of Ryk ICD (nls-Ryk ICD), element described above, that is under the control of a doxycycline-repressible TET element, tTA^2S. This allows us to titer the levels of expression of activated Ryk by varying the concentration of doxycycline introduced in culture during differentiation (Figure 6B; see STAR Methods). Previous work from our lab has shown that cortical interneurons derived from this system develop normally *in vivo* (Au et al., 2013). When transplanted into the MGE of an embryonic host, they migrate, integrate, and mature in a manner indistinguishable from their endogenous counterparts. This allows for the postnatal *in vivo* analysis of mature ES-cell-derived interneurons. In the absence of doxycycline, nls-Ryk ICD is expressed at maximum levels. This resulted in virtually all ES-cell-derived interneurons adopting an SST+ identity (91% SST+, 9% PV+, n = 4). The addition of a low concentration of doxycycline partially depressed the levels of induced nls-Ryk ICD and resulted in an increased number of PV+ cortical interneurons being produced (50% SST+, 50% PV+, n = 3, p = 0.001, paired Student's t test compared with no doxycycline condition). Higher levels of doxycycline further decreased nls-Ryk ICD levels and resulted in the production of proportionally more PV+ interneurons and fewer SST+ cells (34% SST+, 66% PV+, n = 4, p = 0.03, paired Student's t test compared with no doxycycline condition) (Figure 6C). These data indicate that Ryk signaling influences the proportion of PV+ versus SST+ interneurons on a population level by controlling the amount of SST+ interneurons produced in a graded fashion.

DISCUSSION

In this study, we describe a caudal to rostral axis in Wnt responsiveness within the MGE. The production of SST+ and PV+ cortical interneurons parallels this axis: SST+ cells originate in

the caudal MGE in close proximity to Wnt, and PV+ cells arise from the rostral MGE distal to the Wnt source. We find that Wnt-responsive cells from the MGE overwhelmingly become SST+ interneurons and that Wnt is required for a population bias in cIN identity. We further demonstrate that the non-canonical Wnt receptor Ryk plays an active role in specifying SST+ fate through its intracellular domain. Activation of the Ryk pathway in MGE progenitors biases cells toward SST+ identity. Importantly, MGE-specific genetic loss of *Ryk* function results in a large proportion of both PV+ and SST+ cells failing to acquire subtype identity. Together, these data suggest that while high levels of Ryk signaling drive the normal generation of SST+ interneurons, low levels of Ryk signaling are required for the generation of a large proportion of PV+ interneurons. Consistent with this notion, we demonstrate that graded levels of Ryk signaling, through nuclear localization of Ryk ICD, regulate the proportions of SST+ and PV+ cINs produced from an ES- cell-based model system of interneuron development. These data strongly suggest that Ryk signaling is a key component in mediating interneuron subclass specification and acts in a graded fashion to regulate the proportions of interneuron subclasses produced over developmental time.

Our findings are in accordance with observed differences of gene expression across spatial subdomains of the MGE (Flames et al., 2007). Previous studies also indicate spatial biases in the cell types produced in different MGE subdomains (Wonders et al., 2008; Hu et al., 2017). These studies have largely focused on the dorsal-ventral axis along the MGE. For instance, findings from the Anderson laboratory have implicated Shh signaling in regulating the specification of SST+ versus PV+ interneurons (Tyson et al., 2015; Xu et al., 2005, 2010). Recent work has also described rostral-caudal MGE transcription factor subdomains (Hu et al., 2017). For simplicity, we have referred to the regional variability described here as being oriented caudal to rostral. More precisely, it is based on progenitor cell proximity to Wnt, likely emanating from the thalamus, which is located dorsally and toward the caudal midline relative to the MGE. As such, our results are consistent with previous studies reporting SST+ interneurons and PV+ interneurons preferentially derived from dorsal MGE and ventral MGE, respectively (Wonders et al., 2008). In an attempt to reconcile the previously reported role of Shh signaling in interneuron subclass specification, we pharmacologically attenuated Shh by intraventricular cyclopamine injection at E12.5. While this resulted in a decrease in Gli1 expression in the MGE, it did not alter PV and SST numbers at P21 in Ryk wild-type animals. Further, it did not exacerbate the phenotype in Ryk mutants, where the number of unidentified cells was unaffected. These data suggest that Shh regulation of interneuron identity likely occurs prior to E12.5 when cyclopamine was administered. Critically, it also suggests that in the absence of Ryk signaling, Shh does not serve a redundant role to establish interneuron identity in the PV and SST cells that retain marker expression.

In the MGE, Wnt signaling appears to play multiple roles. While canonical Wnt signaling is critical for MGE expansion (Gulacsi and Anderson, 2008), we found that genetic ablation of β-catenin in the MGE results in little change in the relative proportion of different interneuron subtypes. Interestingly, these data suggest that Wnt proliferative and specification functions can be deconvolved, potentially along different signaling pathways. Importantly, canonical Wnt loss of function results in a trend of decreased PV+ interneurons, in accordance with studies suggesting that PV+ cell progenitors preferentially undergo transit amplification and thus are likely more sensitive to proliferative manipulations (Glickstein et al., 2007; Petros et al., 2015). Similarly, Ryk activity plays a role in directing the mode of neurogenesis adopted by cortical progenitors (Lyu et al., 2008). Therefore, Shh, canonical Wnt, and non-canonical Wnt signaling may participate in both proliferation and patterning across developmental timescales. Loss of Shh signaling in MGE progenitors at E10.5 results in changes in interneuron production (Xu et al., 2010). By contrast, we have demonstrated that cyclopamine treatment at E12.5 does not significantly affect interneuron fate specification, suggesting that Shh morphogenic effects occur predominantly at earlier time points. Conversely, treatment of embryos at E12.5 with the Wnt inhibitor IWP2 results in a significant fate switch in interneuron subclasses. Collectively, our data suggest that Wnt signaling shifts from a predominantly proliferative to a fate-determinative role over developmental time. Thus, there remains the intriguing possibility for overlap in the effects of Wnt and Shh signaling as they impinge on the mode of neurogenesis and proliferation rates during early MGE patterning.

In addition to its role in regulating proliferation, Wnt is a well-known determinant of cell fate in both invertebrates and vertebrates. Within the nervous system, Wnt has an early role as a dorsalizing factor during early stages of development (reviewed in Lee and Jessell, 1999).

The present findings indicate a later role for Wnt signaling in forebrain patterning, as a secondary gradient emanating from dorso-caudal signaling sources. Importantly, these data highlight the utility of considering the forebrain in three dimensions and the constantly evolving spatial relationship between neighboring structures. Much like the notochord induces the nearby floorplate in the developing spinal cord (Placzek et al., 2000), the gradient we describe here is a reflection of how spatially positioned co-developing structures are important sources of developmental signals.

Wnt-Ryk signaling via the planar cell polarity pathway has been previously implicated in neuronal development (Hollis et al., 2016; Lanoue et al., 2017; Macheda et al., 2012; Nüsslein-Volhard and Wieschaus, 1980; Reynaud et al., 2015; Schmitt et al., 2006). A number of other studies have found that translocation of the Ryk intracellular domain to the nucleus in response to Wnt activity directs progenitor cell neurogenesis in the developing dorsal and ventral forebrain (Chang et al., 2017; Kamitori et al., 2005; Lyu et al., 2008; Zhong et al., 2011). Our findings also suggest that Ryk ICD signaling plays an important role in interneuron subtype identity. Conditional loss of function of Ryk in the MGE (*Nkx2.1*^{Cre}; *Ryk*$^{f/f}$) resulted in a dramatic decrease in specified interneurons and equal proportions of PV+ and SST+ cells, a pronounced departure from their normal 65:35 ratio. Notably, transplantation of *Ryk*$^{-/-}$ MGE replicated our findings by genetic loss of function, bolstering the notion that MGE transplantation is a valid approach where conditional loss-of-function allele is unavailable.

Overall, our loss-of-function analysis indicates that Ryk signaling is crucial for the specification of both PV+ and SST+ interneurons. Interestingly, Ryk loss-of-function progenitors are capable of generating specified cells, although without the normal ratio observed in wild-type interneurons. These data suggest the presence of redundant systems that allow for the production of PV+ and SST+ interneurons (albeit with many unspecified cells) in the absence of Ryk signaling. Importantly, we observed that PV and SST interneuron identity is not affected when Ryk is ablated postmitotically with either *Dlx6a*^{Cre} or *SST*^{Cre} driver lines. This indicates that the influence of Ryk signaling in subclass identity is confined to the MGE progenitor stage, consistent with previous findings (Butt et al., 2008).

We hypothesize that Ryk signaling stochastically biases nascent interneuron subtype identity as they become postmitotic. In this scenario, graded levels of Ryk signaling act to fine-tune and regulate MGE output in order to generate the appropriate numbers of PV+ and SST+ interneurons. We directly tested this hypothesis by using our previously established *in vitro* model system of interneuron development (Au et al., 2013). This enabled us to modulate the ratio of PV+/SST+ interneurons by varying the levels of Ryk ICD signaling in a doxycycline dose-dependent fashion. These data strongly support the idea that Ryk ICD signaling acts in a graded manner to determine cell-fate decisions in the MGE.

Interneurons undergo a protracted period of development from the time of their generation to full maturity. The phenotypes observed in our analysis of conditional Ryk loss of function and grafting analysis of *Ryk*$^{-/-}$ MGE suggest that in addition to playing a role in fate selection, *Ryk* may also contribute to interneuron maturation. In this study, we have limited our analysis to MGE neurogenesis. This is the period that we have previously hypothesized is critical for cardinal specification of cell type. Subsequently, through a process we have termed definitive specification, interneuron fate is likely refined during both their migration and upon reaching their settling position (Kepecs and Fishell, 2014). Later aspects of interneuron maturation might also be influenced by the level of Ryk activity. Exploring these roles is an appealing area for future investigation. Higher throughput methods such as ES cell differentiation and transplantation may prove to be an effective approach to further study *Ryk*-dependent phenotypes in greater detail during these later phases. Regardless of its further roles, our findings indicate that Ryk signaling mediates morphogenetic signaling influencing the production of both PV+ and SST+ interneurons from MGE progenitor pools.

STAR★METHODS

Detailed methods are provided in the online version of this paper and include the following:

- KEY RESOURCES TABLE
- LEAD CONTACT AND MATERIALS AVAILABILITY
- EXPERIMENTAL MODEL AND SUBJECT DETAILS
  - Animal husbandry
  - Cell culture
- METHOD DETAILS
  - Protein Analysis
  - Immunohistochemistry
  - *In situ* Hybridization
  - Ultrasound guided *in utero* transplantation
  - In utero injections and electroporation
  - Rostral/caudal MGE dissections
  - Wnt signaling reporter fate-mapping
- QUANTIFICATION AND STATISTICAL ANALYSIS
- DATA AND CODE AVAILABILITY

SUPPLEMENTAL INFORMATION

Supplemental Information can be found online at https://doi.org/10.1016/j.neuron.2019.06.003.

ACKNOWLEDGMENTS

The authors wish to thank Kat Hadjantonakis and Wange Lu for generous donation of Tcf/Lef:H2B-dGFP and *Ryk*$^{-/-}$ animals, respectively; Andre Goffinet for guidance on *Vangl2* mutants; Dhananjay Bambah-Mukku and Marian Fernandez Otero of the Dulac and Fishell laboratories, respectively, for RNAscope protocol advice and reagents; and Zhimin Lao and Alexandra Joyner for helpful discussions about Shh signaling and performing Gli1 *in situ* hybridization. This work was supported by the following NIH grants: F30 MH087045 (M.G.M.), T32 MH015174-40 (M.G.M.), R01-NS081297 (G.J.F.), R01-MH071679 (G.J.F.), P01-NS074972 (G.J.F.), as well as generous support from the Simons Foundation (G.J.F.) and the Whitehall Foundation (E.A.). M.G.M. was supported by the NYU Medical Scientist Training Program.

AUTHOR CONTRIBUTIONS

M.G.M. conducted and analyzed the majority of experiments. L.V.C. conducted analysis of Ryk ICD gain-of-function experiments. P.D.D. performed western blots. T.J.P. conducted electroporation experiments. M.M.H. and S.A.S. assisted with Ryk ICD constructs, Ryk function-blocking antibody, and *Ryk* null mouse. Y.Z. contributed *Ryk* conditional mouse. G.J.F. contributed to experimental design. E.A. and M.G.M. designed experiments and co-wrote the manuscript. E.A. conceived of the study.

DECLARATION OF INTERESTS

The authors declare no competing interests.

Received: December 21, 2017
Revised: April 12, 2019
Accepted: June 6, 2019
Published: June 27, 2019

REFERENCES

Anderson, S.A., Eisenstat, D.D., Shi, L., and Rubenstein, J.L. (1997). Interneuron migration from basal forebrain to neocortex: dependence on Dlx genes. Science *278*, 474–476.

Au, E., Ahmed, T., Karayannis, T., Biswas, S., Gan, L., and Fishell, G. (2013). A modular gain-of-function approach to generate cortical interneuron subtypes from ES cells. Neuron *80*, 1145–1158.

Bai, C.B., Auerbach, W., Lee, J.S., Stephen, D., and Joyner, A.L. (2002). Gli2, but not Gli1, is required for initial Shh signaling and ectopic activation of the Shh pathway. Development *129*, 4753–4761.

Barrott, J.J., Cash, G.M., Smith, A.P., Barrow, J.R., and Murtaugh, L.C. (2011). Deletion of mouse Porcn blocks Wnt ligand secretion and reveals an ectodermal etiology of human focal dermal hypoplasia/Goltz syndrome. Proc. Natl. Acad. Sci. USA *108*, 12752–12757.

Brault, V., Moore, R., Kutsch, S., Ishibashi, M., Rowitch, D.H., McMahon, A.P., Sommer, L., Boussadia, O., and Kemler, R. (2001). Inactivation of the beta-catenin gene by Wnt1-Cre-mediated deletion results in dramatic brain malformation and failure of craniofacial development. Development *128*, 1253–1264.

Briscoe, J., and Ericson, J. (2001). Specification of neuronal fates in the ventral neural tube. Curr. Opin. Neurobiol. *11*, 43–49.

Butt, S.J., Fuccillo, M., Nery, S., Noctor, S., Kriegstein, A., Corbin, J.G., and Fishell, G. (2005). The temporal and spatial origins of cortical interneurons predict their physiological subtype. Neuron *48*, 591–604.

Butt, S.J.B., Sousa, V.H., Fuccillo, M.V., Hjerling-Leffler, J., Miyoshi, G., Kimura, S., and Fishell, G. (2008). The requirement of Nkx2-1 in the temporal specification of cortical interneuron subtypes. Neuron *59*, 722–732.

Cadigan, K.M., and Waterman, M.L. (2012). TCF/LEFs and Wnt signaling in the nucleus. Cold Spring Harb. Perspect. Biol. *4*, 4.

Cardin, J.A., Carlén, M., Meletis, K., Knoblich, U., Zhang, F., Deisseroth, K., Tsai, L.H., and Moore, C.I. (2009). Driving fast-spiking cells induces gamma rhythm and controls sensory responses. Nature *459*, 663–667.

Chang, W.H., Choi, S.H., Moon, B.S., Cai, M., Lyu, J., Bai, J., Gao, F., Hajjali, I., Zhao, Z., Campbell, D.B., et al. (2017). Smek1/2 is a nuclear chaperone and cofactor for cleaved Wnt receptor Ryk, regulating cortical neurogenesis. Proc. Natl. Acad. Sci. USA *114*, E10717–E10725.

Charron, F., and Tessier-Lavigne, M. (2005). Novel brain wiring functions for classical morphogens: a role as graded positional cues in axon guidance. Development *132*, 2251–2262.

Chen, B., Dodge, M.E., Tang, W., Lu, J., Ma, Z., Fan, C.W., Wei, S., Hao, W., Kilgore, J., Williams, N.S., et al. (2009). Small molecule-mediated disruption of Wnt-dependent signaling in tissue regeneration and cancer. Nat. Chem. Biol. *5*, 100–107.

De Marco García, N.V., Karayannis, T., and Fishell, G. (2011). Neuronal activity is required for the development of specific cortical interneuron subtypes. Nature *472*, 351–355.

De Marco García, N.V., Priya, R., Tuncdemir, S.N., Fishell, G., and Karayannis, T. (2015). Sensory inputs control the integration of neurogliaform interneurons into cortical circuits. Nat. Neurosci. *18*, 393–401.

Dehorter, N., Ciceri, G., Bartolini, G., Lim, L., del Pino, I., and Marín, O. (2015). Tuning of fast-spiking interneuron properties by an activity-dependent transcriptional switch. Science *349*, 1216–1220.

Dessaud, E., Yang, L.L., Hill, K., Cox, B., Ulloa, F., Ribeiro, A., Mynett, A., Novitch, B.G., and Briscoe, J. (2007). Interpretation of the sonic hedgehog morphogen gradient by a temporal adaptation mechanism. Nature *450*, 717–720.

Ericson, J., Briscoe, J., Rashbass, P., van Heyningen, V., and Jessell, T.M. (1997). Graded sonic hedgehog signaling and the specification of cell fate in the ventral neural tube. Cold Spring Harb. Symp. Quant. Biol. *62*, 451–466.

Ferrer-Vaquer, A., Piliszek, A., Tian, G., Aho, R.J., Dufort, D., and Hadjantonakis, A.K. (2010). A sensitive and bright single-cell resolution live imaging reporter of Wnt/ß-catenin signaling in the mouse. BMC Dev. Biol. *10*, 121.

Fino, E., and Yuste, R. (2011). Dense inhibitory connectivity in neocortex. Neuron *69*, 1188–1203.

Fishell, G., and Rudy, B. (2011). Mechanisms of inhibition within the telencephalon: "where the wild things are". Annu. Rev. Neurosci. *34*, 535–567.

Flames, N., Pla, R., Gelman, D.M., Rubenstein, J.L., Puelles, L., and Marín, O. (2007). Delineation of multiple subpallial progenitor domains by the combinatorial expression of transcriptional codes. J. Neurosci. *27*, 9682–9695.

Glickstein, S.B., Moore, H., Slowinska, B., Racchumi, J., Suh, M., Chuhma, N., and Ross, M.E. (2007). Selective cortical interneuron and GABA deficits in cyclin D2-null mice. Development *134*, 4083–4093.

Green, J., Nusse, R., and van Amerongen, R. (2014). The role of Ryk and Ror receptor tyrosine kinases in Wnt signal transduction. Cold Spring Harb. Perspect. Biol. *6*, 6.

Gulacsi, A.A., and Anderson, S.A. (2008). Beta-catenin-mediated Wnt signaling regulates neurogenesis in the ventral telencephalon. Nat. Neurosci. *11*, 1383–1391.

Halford, M.M., Armes, J., Buchert, M., Meskenaite, V., Grail, D., Hibbs, M.L., Wilks, A.F., Farlie, P.G., Newgreen, D.F., Hovens, C.M., et al. (2000). Ryk-deficient mice exhibit craniofacial defects associated with perturbed Eph receptor crosstalk. Nat. Genet. *25*, 414–418.

Halford, M.M., Macheda, M.L., Parish, C.L., Takano, E.A., Fox, S., Layton, D., Nice, E., and Stacker, S.A. (2013). A fully human inhibitory monoclonal antibody to the Wnt receptor RYK. PLoS ONE *8*, e75447.

Hollis, E.R., 2nd, Ishiko, N., Yu, T., Lu, C.C., Haimovich, A., Tolentino, K., Richman, A., Tury, A., Wang, S.H., Pessian, M., et al. (2016). Ryk controls remapping of motor cortex during functional recovery after spinal cord injury. Nat. Neurosci. *19*, 697–705.

Hu, H., Gan, J., and Jonas, P. (2014). Interneurons. Fast-spiking, parvalbumin^{+} GABAergic interneurons: from cellular design to microcircuit function. Science *345*, 1255263.

Hu, J.S., Vogt, D., Lindtner, S., Sandberg, M., Silberberg, S.N., and Rubenstein, J.L.R. (2017). *Coup-TF1* and *Coup-TF2* control subtype and laminar identity of MGE-derived neocortical interneurons. Development *144*, 2837–2851.

Inan, M., Welagen, J., and Anderson, S.A. (2012). Spatial and temporal bias in the mitotic origins of somatostatin- and parvalbumin-expressing interneuron subgroups and the chandelier subtype in the medial ganglionic eminence. Cereb. Cortex *22*, 820–827.

Inan, M., Blázquez-Llorca, L., Merchán-Pérez, A., Anderson, S.A., DeFelipe, J., and Yuste, R. (2013). Dense and overlapping innervation of pyramidal neurons by chandelier cells. J. Neurosci. *33*, 1907–1914.

Joyner, A.L. (2000). Gene Targeting: A Practical Approach (Oxford University Press).

Kamitori, K., Tanaka, M., Okuno-Hirasawa, T., and Kohsaka, S. (2005). Receptor related to tyrosine kinase RYK regulates cell migration during cortical development. Biochem. Biophys. Res. Commun. *330*, 446–453.

Kepecs, A., and Fishell, G. (2014). Interneuron cell types are fit to function. Nature *505*, 318–326.

Kvitsiani, D., Ranade, S., Hangya, B., Taniguchi, H., Huang, J.Z., and Kepecs, A. (2013). Distinct behavioural and network correlates of two interneuron types in prefrontal cortex. Nature *498*, 363–366.

Lanoue, V., Langford, M., White, A., Sempert, K., Fogg, L., and Cooper, H.M. (2017). The Wnt receptor Ryk is a negative regulator of mammalian dendrite morphogenesis. Sci. Rep. *7*, 5965.

Lapray, D., Lasztoczi, B., Lagler, M., Viney, T.J., Katona, L., Valenti, O., Hartwich, K., Borhegyi, Z., Somogyi, P., and Klausberger, T. (2012). Behavior-dependent specialization of identified hippocampal interneurons. Nat. Neurosci. *15*, 1265–1271.

Lee, K.J., and Jessell, T.M. (1999). The specification of dorsal cell fates in the vertebrate central nervous system. Annu. Rev. Neurosci. *22*, 261–294.

Liu, A., Joyner, A.L., and Turnbull, D.H. (1998). Alteration of limb and brain patterning in early mouse embryos by ultrasound-guided injection of Shh-expressing cells. Mech. Dev. *75*, 107–115.

Lovett-Barron, M., Turi, G.F., Kaifosh, P., Lee, P.H., Bolze, F., Sun, X.H., Nicoud, J.F., Zemelman, B.V., Sternson, S.M., and Losonczy, A. (2012). Regulation of neuronal input transformations by tunable dendritic inhibition. Nat. Neurosci. *15*, 423–430, S1–S3.

Lyu, J., Yamamoto, V., and Lu, W. (2008). Cleavage of the Wnt receptor Ryk regulates neuronal differentiation during cortical neurogenesis. Dev. Cell *15*, 773–780.

Macheda, M.L., Sun, W.W., Kugathasan, K., Hogan, B.M., Bower, N.I., Halford, M.M., Zhang, Y.F., Jacques, B.E., Lieschke, G.J., Dabdoub, A., and Stacker, S.A. (2012). The Wnt receptor Ryk plays a role in mammalian planar cell polarity signaling. J. Biol. Chem. *287*, 29312–29323.

Madisen, L., Zwingman, T.A., Sunkin, S.M., Oh, S.W., Zariwala, H.A., Gu, H., Ng, L.L., Palmiter, R.D., Hawrylycz, M.J., Jones, A.R., et al. (2010). A robust

and high-throughput Cre reporting and characterization system for the whole mouse brain. Nat. Neurosci. *13*, 133–140.

Miyoshi, G., Butt, S.J., Takebayashi, H., and Fishell, G. (2007). Physiologically distinct temporal cohorts of cortical interneurons arise from telencephalic Olig2-expressing precursors. J. Neurosci. *27*, 7786–7798.

Nery, S., Fishell, G., and Corbin, J.G. (2002). The caudal ganglionic eminence is a source of distinct cortical and subcortical cell populations. Nat. Neurosci. *5*, 1279–1287.

Nüsslein-Volhard, C., and Wieschaus, E. (1980). Mutations affecting segment number and polarity in Drosophila. Nature *287*, 795–801.

Petros, T.J., Bultje, R.S., Ross, M.E., Fishell, G., and Anderson, S.A. (2015). Apical versus basal neurogenesis directs cortical interneuron subclass fate. Cell Rep. *13*, 1090–1095.

Placzek, M., Dodd, J., and Jessell, T.M. (2000). Discussion point. The case for floor plate induction by the notochord. Curr. Opin. Neurobiol. *10*, 15–22.

Proffitt, K.D., and Virshup, D.M. (2012). Precise regulation of porcupine activity is required for physiological Wnt signaling. J. Biol. Chem. *287*, 34167–34178.

Puelles, L., and Rubenstein, J.L. (2003). Forebrain gene expression domains and the evolving prosomeric model. Trends Neurosci. *26*, 469–476.

Qu, Y., Huang, Y., Feng, J., Alvarez-Bolado, G., Grove, E.A., Yang, Y., Tissir, F., Zhou, L., and Goffinet, A.M. (2014). Genetic evidence that Celsr3 and Celsr2, together with Fzd3, regulate forebrain wiring in a Vangl-independent manner. Proc. Natl. Acad. Sci. USA *111*, E2996–E3004.

Reynaud, E., Lahaye, L.L., Boulanger, A., Petrova, I.M., Marquilly, C., Flandre, A., Martianez, T., Privat, M., Noordermeer, J.N., Fradkin, L.G., and Dura, J.M. (2015). Guidance of Drosophila mushroom body axons depends upon DRL-Wnt receptor cleavage in the brain dorsomedial lineage precursors. Cell Rep. *11*, 1293–1304.

Roelink, H., Porter, J.A., Chiang, C., Tanabe, Y., Chang, D.T., Beachy, P.A., and Jessell, T.M. (1995). Floor plate and motor neuron induction by different concentrations of the amino-terminal cleavage product of sonic hedgehog autoproteolysis. Cell *81*, 445–455.

Roy, J.P., Halford, M.M., and Stacker, S.A. (2018). The biochemistry, signalling and diseaserelevance of RYK and other WNT-binding receptor tyrosine kinases. Growth Factors *36*, 15–40.

Rubenstein, J.L., Martinez, S., Shimamura, K., and Puelles, L. (1994). The embryonic vertebrate forebrain: the prosomeric model. Science *266*, 578–580.

Schmitt, A.M., Shi, J., Wolf, A.M., Lu, C.C., King, L.A., and Zou, Y. (2006). Wnt-Ryk signalling mediates medial-lateral retinotectal topographic mapping. Nature *439*, 31–37.

Sousa, V.H., Miyoshi, G., Hjerling-Leffler, J., Karayannis, T., and Fishell, G. (2009). Characterization of Nkx6-2-derived neocortical interneuron lineages. Cereb. Cortex *19* (*Suppl 1*), i1–i10.

Sussel, L., Marin, O., Kimura, S., and Rubenstein, J.L. (1999). Loss of Nkx2.1 homeobox gene function results in a ventral to dorsal molecular respecification within the basal telencephalon: evidence for a transformation of the pallidum into the striatum. Development *126*, 3359–3370.

Suzuki, K., Bose, P., Leong-Quong, R.Y., Fujita, D.J., and Riabowol, K. (2010). REAP: a two minute cell fractionation method. BMC Res. Notes *3*, 294.

Taniguchi, H., Lu, J., and Huang, Z.J. (2013). The spatial and temporal origin of chandelier cells in mouse neocortex. Science *339*, 70–74.

Tyson, J.A., Goldberg, E.M., Maroof, A.M., Xu, Q., Petros, T.J., and Anderson, S.A. (2015). Duration of culture and sonic hedgehog signaling differentially specify PV versus SST cortical interneuron fates from embryonic stem cells. Development *142*, 1267–1278.

Wamsley, B., and Fishell, G. (2017). Genetic and activity-dependent mechanisms underlying interneuron diversity. Nat. Rev. Neurosci. *18*, 299–309.

Watanabe, K., Kamiya, D., Nishiyama, A., Katayama, T., Nozaki, S., Kawasaki, H., Watanabe, Y., Mizuseki, K., and Sasai, Y. (2005). Directed differentiation of telencephalic precursors from embryonic stem cells. Nat. Neurosci. *8*, 288–296.

Wichterle, H., Turnbull, D.H., Nery, S., Fishell, G., and Alvarez-Buylla, A. (2001). In utero fate mapping reveals distinct migratory pathways and fates of neurons born in the mammalian basal forebrain. Development *128*, 3759–3771.

Willert, K., and Nusse, R. (2012). Wnt proteins. Cold Spring Harb. Perspect. Biol. *4*, a007864.

Willert, K., Brown, J.D., Danenberg, E., Duncan, A.W., Weissman, I.L., Reya, T., Yates, J.R., 3rd, and Nusse, R. (2003). Wnt proteins are lipid-modified and can act as stem cell growth factors. Nature *423*, 448–452.

Wonders, C.P., and Anderson, S.A. (2006). The origin and specification of cortical interneurons. Nat. Rev. Neurosci. *7*, 687–696.

Wonders, C.P., Taylor, L., Welagen, J., Mbata, I.C., Xiang, J.Z., and Anderson, S.A. (2008). A spatial bias for the origins of interneuron subgroups within the medial ganglionic eminence. Dev. Biol. *314*, 127–136.

Xu, Q., Wonders, C.P., and Anderson, S.A. (2005). Sonic hedgehog maintains the identity of cortical interneuron progenitors in the ventral telencephalon. Development *132*, 4987–4998.

Xu, Q., Tam, M., and Anderson, S.A. (2008). Fate mapping Nkx2.1-lineage cells in the mouse telencephalon. J. Comp. Neurol. *506*, 16–29.

Xu, Q., Guo, L., Moore, H., Waclaw, R.R., Campbell, K., and Anderson, S.A. (2010). Sonic hedgehog signaling confers ventral telencephalic progenitors with distinct cortical interneuron fates. Neuron *65*, 328–340.

Zhong, J., Kim, H.T., Lyu, J., Yoshikawa, K., Nakafuku, M., and Lu, W. (2011). The Wnt receptor Ryk controls specification of GABAergic neurons versus oligodendrocytes during telencephalon development. Development *138*, 409–419.

STAR★METHODS

KEY RESOURCES TABLE

REAGENT or RESOURCE	SOURCE	IDENTIFIER
Antibodies		
Rat anti-SST	Millipore	Cat#MAB354 RRID: AB_2255374
Mouse monoclonal anti-Parvalbumin	Sigma	Cat#P3088 RRID: AB_477329
Rabbit anti-VIP	ImmunoStar	Cat#20077 RRID: AB_572270
Mouse anti-CR50	MBL	Cat#D223-3 RRID: AB_843523
Rabbit monoclonal anti Ryk N-term	Abcam	RRID: AB_10973565
Rabbit anti-Ryk C-term	Thermo	RRID: AB_2285487
Rabbit anti-Ryk N-term	Hollis et al., 2016	N/A
Mouse anti Cyclophilin A	Abcam	RRID: AB_879767
Rb anti-histone H3	Cell Signaling	RRID: AB_331563
Mouse anti β-actin	Thermo Fisher	MA5-15739
Chemicals, Peptides, and Recombinant Proteins		
IWP2	Sigma	Cat#686770-61-6
cyclopamine	CalBioChem	Cat#239803
Dikkopf-1	Tocris	Cat#5897-DK/CF
Sonic Hedgehog	Tocris	Cat#464-SH
Ryk function blocking antibody	Halford et al., 2013	N/A
Critical Commercial Assays		
RNAScope	ACDbiosystems	Cat#323100
Experimental Models: Cell Lines		
Dlx6a^{Cre}; Ai9	This paper	N/A
Experimental Models: Organisms/Strains		
Nkx2-1^{Cre}	Xu et al., 2008	JAX: 008661
Ryk$^{-/-}$	Halford et al., 2013	RRID: MGI:2667559
β-catenin$^{f/f}$	Brault et al., 2001	JAX: 004152
Tcf/Lef:H2B-dGFP	Ferrer-Vaquer et al., 2010	RRID: IMSR_JAX:013752
Ai9	Madisen et al., 2010	equivalent: RRID: IMSR_JAX:007914
RCE	Sousa et al., 2009	JAX:32037
TK^{Cre}	Bai et al., 2002	MGI:4437924
Ryk conditional	Hollis et al., 2016	MGI:6147406
Oligonucleotides		
Ryk Primers		N/A
Recombinant DNA		
Nestin-Nkx2-1-IRES-tTA	Au et al., 2013	N/A
Dlx2 – TetO – NLS-RykICD	This paper	N/A
Nestin – LSL – NLS-RykICD	This paper	N/A
pCAG – LSL - eGFP	Petros et al., 2015	N/A

LEAD CONTACT AND MATERIALS AVAILABILITY

Further information and requests for resources and reagents should be directed to Edmund Au (ea2515@cumc.columbia.edu).

EXPERIMENTAL MODEL AND SUBJECT DETAILS

Animal husbandry

All animal handling and maintenance were performed according to the regulations of the Institutional Animal Care and Use Committee of the NYU School of Medicine and Columbia University Medical center. The following lines were genotyped as previously described: *Nkx2-1*^{Cre} (Xu et al., 2008), *Ryk*$^{-/-}$ (Halford et al., 2013) (RRID:MGI:2667559), *β-catenin*$^{f/f}$ (Brault et al., 2001), *Tcf/Lef:H2B-dGFP* (Ferrer-Vaquer et al., 2010) (RRID:IMSR_JAX:013752), *Ai9* (Madisen et al., 2010) (equivalent: RRID:IMSR_JAX:007914), *RCE* (Sousa et al., 2009), and *TK*^{Cre} (Bai et al., 2002). *Ryk* conditional (Hollis et al., 2016) animals were received on a black 6 background (C57B6), mutant progeny were not initially observed when crossed onto *Nkx2.1*^{Cre} (also B6), homozygous mutant productive crosses occurred after outbreeding to the CD-1 background. Wild-type timed pregnant females for transplant recipients, IWP2 or Ryk function blocking antibody experiments were of the Swiss-webster background and ordered from Taconic. All embryonic time points were counted from discovery of vaginal plug (e0.5).

Cell culture

Mouse ES cells were maintained using standard protocols (Joyner, 2000). Low passage cell lines were differentiated using protocols describsed previously (Au et al., 2013; Watanabe et al., 2005). Briefly, ES cells in late log phase growth were dissociated into single cells and plated into non-TC treated wells at a density of 35 000 cells/well in order to establish floating embryoid body (EB) cultures. EBs were successively treated with Dikkopf-1 (2.5 ng/mL), and Sonic Hedgehog (40 ng/mL) for 11-13 days, after which they were gently dissociated (Accutase (Invitrogen), 15′, 37°C) for subsequent experiments. The *RykICD* was generated by PCR using full-length human *RYK* cDNA with a C terminus myc tag (provided by Stephen Stacker, Peter MacCallum Cancer Centre, Melbourne, Australia) as a template and cloning a nuclear localization signal in frame at the N terminus (Lyu et al., 2008). This construct was introduced into a bi-directional tet-responsive element driving Dlx2 in one direction and Ryk ICD in the other (Au et al., 2013). This assembly was then nucleiofected into a *Dlx6a*^{Cre}; Ai9 reporter ES cell line along with Nestin-Nkx2-1-IRES-tTA (Lonza). Individual clones were isolated, expanded, genotyped, and verified by *in vitro* differentiation.

METHOD DETAILS

Protein Analysis

Tissue samples for protein analysis were dissected into rMGE, cMGE or wMGE fractions and processed as below. A minimum of 5 embryos were pooled for each embryonic sample condition. For cell culture protein analysis, embryoid bodies were collected at 11-13 days after differentiation, rinsed with PBS and resuspended in 100 μL of lysis buffer (95mM NaCl, 25mM Tris-HCl pH 7.5, 10mM EDTA and 2% SDS, final pH = 8.0 including protease inhibitor mix (cOmplete Ultra Roche)), and homogenized with a brief pulse using an ultrasonicator with microtip (Misonix S-4000, amplitude = 1, 5 s pulse). Samples destined for fractionation were processed as described (Suzuki et al., 2010). Protein samples were quantified and lanes to be compared loaded with equal amounts of total protein. Blots were probed using an antibody mix and both channels imaged simultaneously with fluorescent secondary antibodies (Li-Cor). The following primary antibodies were used: Rabbit monoclonal anti Ryk N-term (AbCam, 1:50,000, RRID:AB_10973565), Rabbit anti-Ryk C-term (Thermo 1:1000, RRID:AB_2285487), Rabbit anti-Ryk N-term (Zou lab, 1:1000), mouse anti Cyclophilin A (Abcam 1 μg/mL, RRID:AB_879767), Rb anti-histone H3 (Cell Signaling, 1:2000, RRID:AB_331563), mouse anti β-actin (1:2000). Blots were imaged using Odyssey CLx Infared Imager and analyzed using ImageStudio software (Li-Cor). Protein fluorescent signal was normalized to beta actin loading control intensity in whole cell or cytoplasmic fractions, and to histone in nuclear fractions.

Immunohistochemistry

Embryos aged e15.5 or later and adult mice were transcardially perfused with 4% paraformaldehyde in PBS (4%PFA). Tissue was prepared for either cryosectioning and slide staining or vibratome sectioning followed by free-floating immunohistochemistry. Both cryosectioning and vibratome sectioning were used in transplantation experiments (Figures 2, 3, 5, and 6). No difference was found between the two tissue preparations (data not shown) and all non-transplantation experimental analysis was performed in free-floating sections. For cryosectioning, brains were dissected and post-fixed in 4%PFA one h at 4°C, then cryoprotected in 30% sucrose W/V in PBS overnight at 4°C. Prepared brains were mounted in Tissue-Tek (Takara) frozen at −80°C for storage until cryo-sectioned at −20°C in 12 μm sections for embryonic tissue and 20 μm sections for adult tissue. Brains for cryosectioning were transcardially perfused as above and post-fixed in 4%PFA overnight at 4°C. Brains were embedded in 4% low melt agarose in PBS and sectioned to 50 μm on a Leica VT1000S vibratome. Sections were stored in a propylene glycol:glycerol:PBS solution (3:3:4) at −20°C until used. For immunohistochemistry, cryosections were allowed to dry for 1-2 h then frozen at −20°C until they were used. Frozen sections were defrosted and dried at room temperature for 1 h then rehydrated in blocking solution (4% normal serum, 0.1% Triton X-100 in PBS) for 1-4 h. Primary antibody incubation followed in blocking solution overnight at 4°C. Primary antibodies were used at the following concentrations: Rat anti-SST (Millipore 1:500, RRID:AB_2255374), mouse monoclonal anti-Parvalbumin (Sigma 1:1000, RRID:AB_477329), Rabbit anti-VIP (Immunostar 1:1000, RRID:AB_572270), Mouse anti-CR50 (MBL, 1:1000, RRID:AB_843523). Sections were washed repeatedly in PBS then incubated in secondary antibodies conjugated to Alexafluor

488, 594, or 647, host matching serum used for blocking, for 45 min at room temperature. Free-floating sections were incubated in blocking solution (10% serum, 0.3% Triton X-100 in PBS) overnight at 4°C then incubated in primary antibody overnight at 4°C using the antibodies listed above. Free-floating washing steps in PBS were performed overnight or for 4 h at room temperature. When nuclear labeling was desired, DAPI was applied after secondary antibody at 1:10,000 in PBS for 5 min. Slides (free-floating and cryosectioned) were promptly mounted with Fluoromount-G (Southern Biotech) and coverslipped.

In situ Hybridization

Cryosectioned embryonic tissue was prepared for *in situ* hybridization using RNAScope (ACDbiosystems). Protocol was performed using probes for Ryk, Wnt7b, and TCF7L2 as described for Multiplex Fluorescent v2. Tissue permeabilization was achieved through application of Protease III for 30 min.

Ultrasound guided *in utero* transplantation

Ultrasound guided *in utero* transplantation was performed as previously described except where noted below (Au et al., 2013; Liu et al., 1998; Nery et al., 2002; Wichterle et al., 2001). For transplantation of *β-catenin* mutant, plugs were generated from a cross of *Nkx2.1*^{Cre}; *β-catenin*$^{f/+}$ males with *β-catenin*$^{f/f}$; *RCE*$^{f/f}$ females. Homozygous mutant embryos were identified after dissection by midline fusion at the base of the MGE, and tissue samples from the embryo were retained for post hoc genotyping confirmation. Mutant MGE's were dissected and pooled for transplants as above. Ryk$^{-/-}$ embryos could not be identified visually, so pregnant females were deeply anesthetized, and the uterus gently cut to reveal the amniotic sacs. Tail samples were carefully removed from each embryo and rapidly processed for PCR genotyping (as described, Halford et al., 2000), leaving the embryos in place. MGEs were dissected from the identified mutant embryos and processed for transplantation. E13.5 wild-type, unlabeled MGE or LGE tissue was mixed with mutant MGE and used as carrier when little mutant tissue (2 MGEs- 1 null embryo) was available for transplantation.

In utero injections and electroporation

Timed pregnant Swiss Webster females were deeply anesthetized with isofluorane and an incision was made to expose the uterus. IWP2 (sigma) dissolved in DMSO according to manufacturer guidelines, cyclopamine (CalBioChem) was dissolved in ethanol according to manufacturer guidelines, or antibody solution was frontloaded into a beveled glass pipette (as above). 25 nL of IWP2, 50nl of cyclopamine or 100 nL of function-blocking antibody were injected into the ventricles of e12.5 Swiss Webster embryos, the uterus was replaced and the incision stitched, allowing the pups to be born normally or sacrificed 1 day later for MGE collection and transplantation or analysis. Appropriate diluent without chemical was injected as a control. Animals for IWP2 treatment and transplantation experiments were Ai9-germline recombined, wildtype animals were used for function-blocking experiments. Cyclopamine injections were performed on all embryos resultant of *Nkx2.1*^{Cre}; *Ryk*$^{fl/+}$ and *Ryk*$^{fl/+}$ crosses. *In utero* electroporation of the MGE was performed as previously described (Petros et al., 2015). The conditional *Ryk ICD* construct for electroporation was generated as described below (Cell culture) and subcloned downstream of a Nestin promoter and a floxed stop cassette to limit overexpression to the progenitor phase. To allow for post hoc identification a pCAG driven GFP downstream of a floxed stop cassette was co-electroporated, or electroporated alone as control.

Rostral/caudal MGE dissections

Animals expressing a ubiquitous fluorescent marker were generated by crossing either *Ai9* (Madisen et al., 2010) or *RCE* (Sousa et al., 2009) reporter mice with the germline *Cre* driver *TK*^{Cre} (Bai et al., 2002). Pilot experiments were performed using unlabeled SW embryos, dissected MGEs were labeled using a PKH26 Red Fluorescent Cell Linker Mini Kit for General Cell Membrane Labeling (Sigma) following manufacturer's instructions. Ubiquitous fluorescent males were crossed with SW females, and pregnant females were collected at e12.5, morning of vaginal plug discovery counted as e0.5. Embryos were collected and brains were dissected into ice-cold PBS. Cortices were removed and rostral MGE or cMGE was dissected and treated as previously described (Butt et al., 2005). 10-20 embryos were collected and pooled for each condition.

Wnt signaling reporter fate-mapping

Transgenic embryos from timed pregnant Tcf/Lef::H2b-dGFP; pan Ai9+ females were identified under a fluorescent macroscope. Ai9 positive, eGFP negative MGEs and positive MGEs were collected and processed for FACS sorting (Figure S3). Negative MGEs were used for gating. eGFP; Ai9 positive MGEs were dissociated and prepared for FACS sorting following normal cell dissociation methods used for transplantation as described above. Cells were sorted according to expression of eGFP using an iCyt reflection sorter with a 100μM nozzle by the NYU Cytometry and Cell sorting core facility (supported by Perlmutter Cancer Center grant P30CA016087). Collected cells (approximately 9% of cells sorted) were then transplanted into e13 embryos as above.

QUANTIFICATION AND STATISTICAL ANALYSIS

Transplanted cells in cortical areas from sections containing the hippocampus were identified by their expression of the appropriate ubiquitous label (PKH, eGFP or tdTomato) and assessed for their co-expression of SST or PV. Cells were categorized as SST+, PV+

or 'unidentified' (no marker or co-expression of both markers). A minimum of 200 cells were counted per brain, from areas distributed across multiple anterior-posterior sections. Ratios of PV or SST were calculated out of 'unidentified' cells (PV+ or SST+). Ratios in each brain are reported as a single n, and compared across conditions in GraphPad prism software through unpaired Student's t test or chi-square test as noted. In cases where reporter expression was not available (cyclopamine experiments), stained 50μM sections were imaged at 40x using a tiling microscope and absolute numbers of stained cells were counted for a standardized volume spanning all cortical layers.

DATA AND CODE AVAILABILITY

The published article includes all datasets generated and analyzed during this study.